Missouri University of Science and Technology

Electrical and Computer Engineering Faculty Research & Creative Works

Electrical and Computer Engineering

01 May 2001

Modeling DC Power-Bus Structures with Vertical Discontinuities using a Circuit Extraction Approach Based on a Mixed-Potential Integral Equation

Jun Fan
Missouri University of Science and Technology, jfan@mst.edu

Hao Shi

Antonio Orlandi

James L. Knighten

et. al. For a complete list of authors, see https://scholarsmine.mst.edu/ele_comeng_facwork/1733

Recommended Citation

Modeling DC Power-Bus Structures with Vertical Discontinuities Using a Circuit Extraction Approach Based on a Mixed-Potential Integral Equation Formulation

Jun Fan, *Member, IEEE*, Hao Shi, *Member, IEEE*, Antonio Orlandi, *Senior Member, IEEE*, James L. Knighten, *Senior Member, IEEE*, and James L. Drewniak, *Senior Member, IEEE*

Abstract—The dc power-bus is a critical aspect in high-speed digital circuit designs. A circuit extraction approach based on a mixed-potential integral equation is presented herein to model arbitrary multilayer power-bus structures with vertical discontinuities that include decoupling capacitor interconnects. Green's functions in a stratified medium are used and the problem is formulated using a mixed-potential integral equation approach. The final matrix equation is not solved, rather, an equivalent circuit model is extracted from the first-principles formulation. Agreement between modeling and measurements is good, and the utility of the approach is demonstrated for dc power-bus design.

Index Terms—Circuit extraction, decoupling, mixed-potential integral equation, power-bus design, via modeling.

I. INTRODUCTION

A DC POWER structure in a multilayer printed circuit board (PCB) that employs two or more planes as dc power and ground is common in high-speed digital design. Simultaneous switching noise, which can lead to faulty switching, also results in high-frequency noise propagating on the power/ground plane that can cause electromagnetic interference (EMI) problems [1], [2]. Surface-mount technology (SMT) decoupling capacitors are often placed in proximity to high-speed switching devices to mitigate simultaneous switching noise, and reduce the RF noise propagating on the power planes. This method is very effective in many high-speed digital designs [2]–[4]; however, no proven, methodical design guidelines exist for SMT decoupling in dc power bus design. Current practices use a combination of hueristic design guidelines and full-wave modeling to guide SMT capacitor placement and ascertain the effectiveness over frequency. Ultimately, though, achieving a design that meets signal integrity (SI) and EMI requirements is still largely a trial-and-error process. As clock speeds and edge rates increase, meeting requirements in this fashion becomes more difficult and less practical. Further, as design densities increase, flexibility for EMI retrofits late in the design cycle is severely reduced. Guidelines for developing a dc power bus design, as well as evaluating the design are needed. Desirable power bus design guidelines should address several basic issues. These issues include the selection of dielectric material and the interplane capacitance. The total value of SMT decoupling capacitors needed to sufficiently reduce high frequency noise on power planes for the specified active components must be determined. Also, the individual SMT decoupling capacitor value(s) and package(s) must be selected. Further, the SMT decoupling capacitor location relative to specific ICs must be determined. Finally, the printed circuit board layer stackup must be determined, and trade-offs between closely spaced power and ground layers to increase interplane capacitance, and widely spaced planes to accommodate intervening layers and shielding of high-speed signals must be weighed. Hardware trial-and-error can provide insight for a specific design, albeit at development cost and schedule penalties. A general power-bus modeling approach is a powerful design tool that can be integrated into the design process to provide insight with more flexibility than possible with hardware trial-and-error.

The simplest model for a power-bus is a lumped capacitance, since the two planes behave like a parallel-plate capacitor at low frequencies. All SMT decoupling capacitors are then modeled as lumped series RLC circuits, in parallel with the power-bus interplane capacitance, where L and R are parasitic parameters associated with the interconnects and the package [5], [6]. This model is appropriate when the frequency is below board resonance frequencies, which are determined by board dimensions, (typically, several hundred megahertz). Other models, such as a wire-antenna [7], a radial transmission line or rectangular cavity [8]–[11], can partially recover the power-bus distributed behavior neglected by the lumped element modeling of the parallel planes. Other numerical electromagnetic techniques such as FDTD [12] and FEM [13] can be applied to dc power bus design issues, however, device models are not easily accommodated in these approaches. Another class of modeling approaches are *equivalent-circuit models*, by which the system behavior may be modeled in terms of a collection of equivalent circuit elements. An advantage of this approach is that it can easily incorporate well-developed SPICE source, load, and
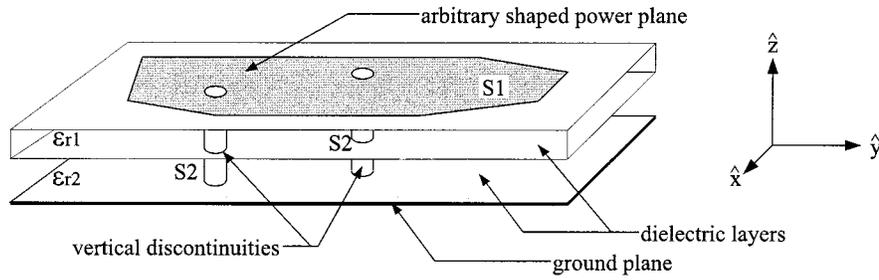
Fig. 1. Power-bus structure with vertical discontinuities.

transmission line models, and it is reusable for multiple simulations in pursuing "what-if" scenarios. Developed circuit extraction techniques include the partial element equivalent circuit (PEEC) method [14]–[16], the transmission line matrix (TLM) method [17], and other transmission-line type approaches [18], [19].

The method proposed in this paper, denoted CEMPIE, is a *C*ircuit *E*xtraction approach based on a *M*ixed-*P*otential *I*ntegral *E*quation [20]. CEMPIE is an extension of the PEEC method to general multilayer dielectric media. Dielectrics can be taken into account in PEEC [15], where finite dielectrics can be treated in a volume-integral formulation. CEMPIE handles infinite dielectric layers. It employs Green's functions for a multi-layered medium; thus, the difficulties and complexity of a volume integral equation formulation that results from an inhomogeneous medium can be transfered to the calculation of Green's functions. Although these Green's functions are tedious to formulate, their calculation is relatively fast. A triangular mesh is adopted so that typical complex contours encountered in PCB design can be modeled. All conductors are assumed of zero thickness, and skin effect loss is neglected in this paper, though skin effect and dielectric losses can be included [21]. One result is provided that includes dielectric losses.

SMT decoupling capacitors added to the PCB to mitigate simultaneous switching noise is an integral part of many dc power-bus designs. These capacitors are connected to the power or ground layer through short traces and vias (interconnects). The parasitic inductance associated with these interconnects limits the SMT capacitor's performance with increasing frequency. In addition, the mutual inductive coupling between two adjacent vias, *e.g.*, the IC and an SMT capacitor, greatly affects the decoupling behavior [22]. Characterizing these vertical discontinuities, in combination with the planar power-bus structure, is necessary for a better understanding of the physics, as well as developing engineering design methodologies. A lumped circuit model for vertical discontinuities, derived from measurements [23], can be incorporated into the equivalent circuit model of a planar power-bus geometry. However, some compensation must be considered to ensure the correctness of the modeling [24]. This paper presents an integral equation formulation, including vertical discontinuities of the SMT via interconnects to avoid such hueristic modeling approaches. A circuit model is extracted that includes all interactions. The mixed-potential integral equation (MPIE) formulation is detailed in Section II, and the circuit extraction procedure

presented in Section III. Calculation of the Green's functions are outlined in Section IV, and modeling and measurement results are compared in Section V.

II. MPIE FORMULATION

The CEMPIE approach is based on an MPIE formulation, from which an equivalent circuit is extracted instead of solving the matrix equation. Similar to the formulation of classic scattering problems, an incident electric field $\vec{E}^{\text{inc}}$ is assumed. Then, surface current densities $\vec{J}(\vec{r})$ and surface charge densities $\sigma(\vec{r})$ are induced on the conducting planes of concern (power planes), and on the surfaces of vertical discontinuities as a result of the incident field. Ground planes and dielectric layers are assumed to be infinite in the modeling, and are incorporated into the Green's functions. When the boundary conditions on the remaining conducting surfaces are enforced, an electric field integral equation results

$$\hat{n} \times \left[j\omega \int_{S1+S2} \bar{\bar{G}}^A(\vec{r}, \vec{r}') \cdot \vec{J}(\vec{r}') ds' + \nabla\phi(\vec{r}) \right] = 0,$$
$$\vec{r} \in S1 + S2, \tag{1}$$

where
- $\bar{\bar{G}}^A$ dyadic Green's function for the vector magnetic potential;
- ϕ induced scalar electric potential;
- $S1$ horizontal planes of concern;
- $S2$ vertical surfaces of vias and/or ports, as shown in Fig. 1.

The incident electric field $\vec{E}^{\text{inc}}$ is assumed to be zero in (1), since an equivalent circuit is extracted from this equation. Thus, excitations can be included in circuit simulators as impressed current sources, which are more easily handled than the incident electric field.

Since triangular patches are more amenable than orthogonal patches in dealing with arbitarily shaped structures, they are chosen to discretize the horizontal planes of concern. However, rectangular patches are used on the vertical surfaces, because, on these vertical surfaces, the axial surface currents are dominant (the height of vias and ports of interest is relatively small). The current vector basis functions are anchored by the interior edges of all triangular surface patches [25]. As illustrated in Fig. 2(a), the nth interior edge has a length of l_n, which uniquely defines two adjacent triangles T_n^+ and T_n^-. Assuming the areas of these two triangles are A_n^+ and A_n^-, and the corresponding free ver-
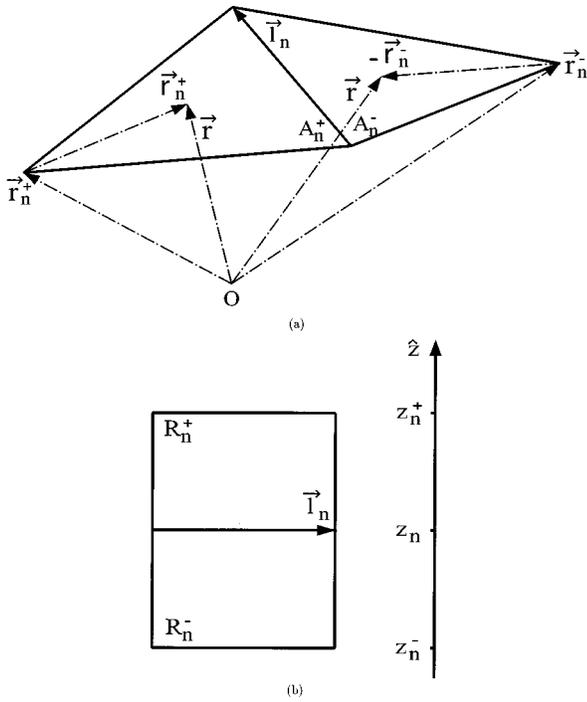
(a)

(b)

Fig. 2.   Basis functions for a triangular or a rectangular mesh.

Fig. 3.   Geometry for intersection edges between triangular and rectangular cells.

tices are $\vec{r}_n^+$ and $\vec{r}_n^-$, then

$$
\vec{f}_n^h(\vec{r}) = \begin{cases} \frac{1}{h_n^+}(\vec{r} - \vec{r}_n^+), & \text{if } \vec{r} \in T_n^+, \\ -\frac{1}{h_n^-}(\vec{r} - \vec{r}_n^-), & \text{if } \vec{r} \in T_n^-, \\ 0, & \text{otherwise} \end{cases}
$$

$$
= \begin{cases} \frac{l_n}{2A_n^+}\vec{\rho}_n^+, & \text{if } \vec{r} \in T_n^+, \\ \frac{l_n}{2A_n^-}\vec{\rho}_n^-, & \text{if } \vec{r} \in T_n^-, \\ 0, & \text{otherwise} \end{cases} \tag{2}
$$

where

f	basis function;
superscript h	basis function is defined for the horizontal triangular cells;
h_n^+	$2A_n^+/l_n$;
h_n^-	$2A_n^+/l_n$;
$\vec{\rho}_n^+$	$\vec{r} - \vec{r}_n^+$;
$\vec{\rho}_n^-$	$\vec{r}_n^- - \vec{r}$.

Since the horizontal components of the surface current densities on the surfaces of vertical discontinuities are assumed to be neglegible, which is the case within the frequency band of interest, the corresponding current basis functions associated with vertical rectangular cells are chosen to have the form of one-dimensional linear functions, and associated only with horizontal edges of rectangles. As shown in Fig. 2(b), l_n is the length of the nth horizontal edge, which uniquely defines two adjacent rectangles R_n^+ and R_n^- with areas of A_n^+ and A_n^-, respectively. Then the current basis function associated with this edge is defined as

$$
\vec{f}_n^v(z) = \begin{cases} \frac{l_n}{A_n^+}(z - z_n^+)\hat{z}, & \text{if } \vec{r} \in R_n^+, \\ \frac{l_n}{A_n^-}(z_n^- - z)\hat{z}, & \text{if } \vec{r} \in R_n^-, \\ 0, & \text{otherwise} \end{cases} \tag{3}
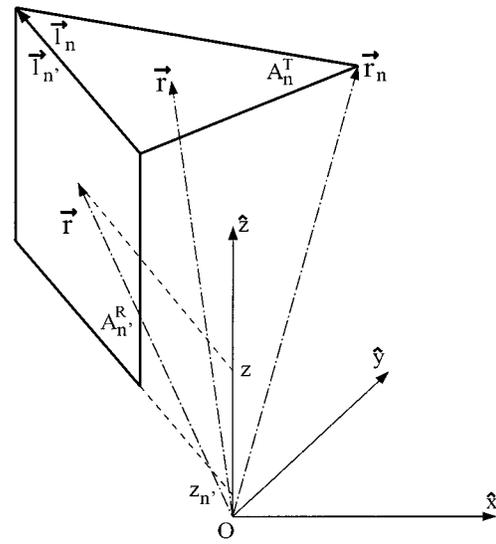$$

where the superscript v indicates that the basis function is defined for the vertical rectangular cells.

For an intersection edge between the horizontal and vertical cells, a triangle and a rectangle are uniquely defined, instead of two triangles or two rectangles. In this case, two *pseudo* edges are assumed for every intersection edge, one belongs to the adjacent triangle, and another belongs to the adjacent rectangle, as shown in Fig. 3. Then, two current densities, one horizontal current density for the triangle, and one vertical current density for the rectangle, are defined and associated with each pseudo edge. These two current densities have the similar formats as in (2) and (3), although they both have only one component rather than two. This treatment of intersections requires an extra step to enforce current continuity after the moment matrix has been filled.

The current basis functions chosen have several important properties. The current component normal to the boundary of the arbitrary-shaped power plane is zero by definition; hence, no line charge exists along the planar boundary. Then, the current component normal to the vertical edges of the rectangular cells is also zero, *i.e.*, no line charge exists along these vertical edges. Furthermore, the current component normal to the edge of any inner triangle is unity everywhere on the edge, which ensures that there is no line charge along this edge. Similarly, the current component normal to any horizontal edge of the rectangular cells is also unity everywhere on the edge. This ensures there is no line charge along the inner horizontal edges of rectangular cells. Finally, it can be shown that the surface charge densities are constant over each cell by taking the surface divergence of these current basis functions.

The induced surface current densities can be expanded using the chosen current basis functions as

$$
\vec{J}_h(\vec{r}) = \sum_{n=1}^{M1} \frac{i_n^h}{l_n} \vec{f}_n^h(\vec{r}),
$$

$$
\vec{J}_v(z) = \sum_{n=M1+1}^{M1+M2} \frac{i_n^v}{l_n} \vec{f}_n^v(z) \tag{4}
$$

where

$M1$ number of all inner edges of the triangular mesh, plus the number of the intersection edges between the triangular and retangular cells;

$M2$ number of all horizontal edges of the rectangular mesh;

i_n unknown current associated with the nth edge.

The dyadic Green's function $\bar{\bar{G}}^A$ in (1) has four components in a stratified medium [26],

$$\bar{\bar{G}}^A = G_{xx}^A(\hat{x}\hat{x} + \hat{y}\hat{y}) + G_{zx}^A\hat{z}\hat{x} + G_{zy}^A\hat{z}\hat{y} + G_{zz}^A\hat{z}\hat{z} \qquad (5)$$

where

G_{zx}^A, G_{zy}^A induced z-directed vector potentials due to an x-oriented or a y-oriented dipole;

G_{xx}^A induced x-directed vector potential due to an x-oriented dipole;

G_{zz}^A induced z-directed vector potential due to a z-directed dipole.

Issues on Green's functions will be further discussed in Section IV. Then, (1) can be decoupled into two equations, when the dyadic Green's function is expanded as in (5), as

$$\int_{s1} G_{xx}^A(\vec{r}, \vec{r}')\vec{J}_h(\vec{r}')ds' + \frac{1}{j\omega}\nabla_{xy}\phi(\vec{r}) = 0, \quad \text{if } \vec{r} \in S1,$$

$$\int_{s1} \left[G_{zx}^A(\vec{r}, \vec{r}')J_x(\vec{r}') + G_{zy}^A(\vec{r}, \vec{r}')J_y(\vec{r}') \right] ds'$$

$$+ \int_{s2} G_{zz}^A(\vec{r}, \vec{r}')J_v(z')ds' + \frac{1}{j\omega}\frac{\partial\phi(\vec{r})}{\partial z} = 0, \quad \text{if } \vec{r} \in S2 \qquad (6)$$

where $\vec{J}_h(\vec{r}') = J_x(\vec{r}')\hat{x} + J_y(\vec{r}')\hat{y}$, and, $\vec{J}_v(z') = J_v(z')\hat{z}$. Equation (6) is then discretized. The surface current densities are expanded using the current basis functions as in (4), and (6) is tested using the functions $\vec{t}^h$ and $\vec{t}^v$ that take the same forms as basis functions defined in (2) and (3). This testing procedure ensures that the inner product reactions on the left-hand side of (6) lead to a symmetric impedance matrix [27], [28]. The moment equation is then expressed as

$$\sum_{n=1}^{M1} \frac{i_n^h}{l_n}\left\langle \vec{t}_{n'}^h, G_{xx}^A * \vec{f}_n^h \right\rangle + \frac{1}{j\omega}\left\langle \vec{t}_{n'}^h, \nabla_{xy}\phi \right\rangle = 0,$$

$$n' = 1, \ldots, M1,$$

$$\sum_{n=1}^{M1} \frac{i_n^h}{l_n}\left[\left\langle t_{n'}^v, G_{zx}^A * \vec{f}_n^h \cdot \hat{x} \right\rangle + \left\langle t_{n'}^v, G_{zy}^A * \vec{f}_n^h \cdot \hat{y} \right\rangle \right]$$

$$+ \sum_{n=M1+1}^{M1+M2} \frac{i_n^v}{l_n}\left\langle t_{n'}^v, G_{zz}^A * f_n^v \right\rangle + \frac{1}{j\omega}\left\langle t_{n'}^v, \frac{\partial\phi}{\partial z} \right\rangle = 0,$$

$$n' = M1+1, \ldots, M1+M2 \qquad (7)$$

where $\vec{t}^v = t^v\hat{z}$ and $\vec{f}^v = f^v\hat{z}$. Notice that $\langle \vec{t}_{n'}^h, G_{xx}^A * \vec{f}_n^h \rangle$ is not a complete reaction between a source and field, rather, it is only a part of it. Therefore, it is not in general equal to $\langle \vec{t}_n^h, G_{xx}^A * \vec{f}_{n'}^h \rangle$.

Based on an assumption that the scalar potential in each cell is constant [29], it can be shown that

$$\left\langle \vec{t}_{n'}^h, \nabla_{xy}\phi \right\rangle = -l_{n'}\left(\phi_{T_{n'}^+} - \phi_{T_{n'}^-} \right),$$

$$n' = 1, \ldots, M1,$$

$$\left\langle t_{n'}^v, \frac{\partial\phi}{\partial z} \right\rangle = -l_{n'}\left(\phi_{R_{n'}^+} - \phi_{R_{n'}^-} \right),$$

$$n' = M1+1, \ldots, M1+M2 \qquad (8)$$

where ϕ is the unknown cell scalar electric potential, which is constant within a cell as assumed. Substituting (8) into (7) results in the matrix equation

$$j\omega \begin{bmatrix} \mathbf{L}^{hh} & 0 \\ \mathbf{L}^{vh} & \mathbf{L}^{vv} \end{bmatrix}\begin{bmatrix} \mathbf{i}^h \\ \mathbf{i}^v \end{bmatrix} - [\mathbf{\Lambda}]\begin{bmatrix} \boldsymbol{\phi}^h \\ \boldsymbol{\phi}^v \end{bmatrix} = 0, \qquad (9)$$

where

$$L_{n'n}^{hh} = \frac{1}{4}\left(M_{n'+n+}^{hh} - M_{n'+n-}^{hh} - M_{n'-n+}^{hh} + M_{n'-n-}^{hh} \right),$$

$$n, n' = 1, \ldots, M1,$$

$$L_{n'n}^{vh} = \frac{1}{2}\left(M_{n'+n+}^{vh} - M_{n'+n-}^{vh} - M_{n'-n+}^{vh} + M_{n'-n-}^{vh} \right),$$

$$n = 1, \ldots, M1, \quad n' = M1+1, \ldots, M1+M2,$$

$$L_{n'n}^{vv} = \left(M_{n'+n+}^{vv} - M_{n'+n-}^{vv} - M_{n'-n+}^{vv} + M_{n'-n-}^{vv} \right),$$

$$n, n' = M1+1, \ldots, M1+M2,$$

$$M_{pq}^{hh} = \frac{1}{A_pA_q}\int_{T_p} ds \int_{T_q} G_{xx}^A(\vec{r}, \vec{r}')\left(\vec{r} - \vec{r}_p^{\mp} \right)\cdot\left(\vec{r}' - \vec{r}_q^{\pm} \right)ds',$$

$$M_{pq}^{vh} = \frac{1}{A_pA_q}\int_{R_p} ds \int_{T_q}\left(z - z_p^{\pm} \right)$$

$$\times\left[G_{zx}^A(\vec{r}, \vec{r}')\vec{\rho}_q(\vec{r}')\cdot\hat{x} + G_{zy}^A(\vec{r}, \vec{r}')\vec{\rho}_q(\vec{r}')\cdot\hat{y} \right]ds',$$

$$M_{pq}^{vv} = \frac{1}{A_pA_q}\int_{R_p} ds \int_{R_q} G_{zz}^A(\vec{r}, \vec{r}')\left(z - z_p^{\pm} \right)\left(z' - z_q^{\pm} \right)ds'. \qquad (10)$$

The positive and negative signs are for positive and negative cells, respectively. $\mathbf{\Lambda}$ is the connectivity matrix between edge-wise quantities and cell-wise quantities, and its elements are determined by

$$\Lambda_{\alpha n} = \begin{cases} 1, & \text{if cell } n \text{ is edge } \alpha\text{'s positive side;} \\ -1, & \text{if cell } n \text{ is edge } \alpha\text{'s negative side;} \\ 0, & \text{otherwise.} \end{cases} \qquad (11)$$

It is important to note here that while the matrix (7) must have a symmetric impedance matrix, separating the equation as in (9) leads to component matrices that by themselves are not symmetric, as is apparent in the $\mathbf{L}$ matrix. This asymmetry must be addressed in the circuit extraction process in order to ensure circuit reciprocity.

In this MPIE formulation, some quantities are edge based such as i^h and i^v, since current basis functions are defined as associated with mesh edges. Others are cell based such as ϕ^h and ϕ^v, because they are assumed constant over each cell. In corresponding circuit notations, an edge is defined as a circuit branch and a cell as a circuit node. Therefore, interpreted in

circuit terms, the above equation is exactly a form of the Kirchoff's voltage law (KVL), *i.e.,* the sum of the voltage drops in a closed loop is zero. The coefficient $j\omega$ before the $\mathbf{L}$ matrix indicates that the matrix represents the inductive behavior of the network. Therefore, it is denoted the *branchwise inductance matrix* herein. This inductance matrix is asymmetric with the right-upper submatrix equal to zero, which is the consequence of the asymmetry in the dyadic Green's function $\bar{\bar{G}}^A$ for the vector potential in a stratified medium. Sommerfeld pointed out that two components of vector potential were required to satisfy the boundary conditions at dielectric interfaces for a horizontal electric dipole [30]. Traditionally [31], for an x- or y-directed electric dipole, the vector potential takes the form

$$\vec{A} = A_h \hat{h} + A_z \hat{z} \tag{12}$$

where h represents x or y. However, for a z-directed electric dipole, the corresponding vector potential only has the z-directional component. For this reason, in the form of $\bar{\bar{G}}^A$ given in (5), there are only G_{zx}^A and G_{zy}^A terms, and no G_{xz}^A and G_{yz}^A terms exist. Any entry in the $\mathbf{L}$ matrix, as discussed before, is only a part of the source-field reaction. Therefore, the asymmetry of the $\mathbf{L}$ matrix does not conflict with the reciprocity theorem. However, it does introduce some difficulties when extracting an equivalent circuit; hence, restoration of symmetry is necessary, and will be discussed later.

On the other hand, *nodal currents* can be defined as total currents flowing out of the corresponding mesh cells. This means that

$$I_n^h = \int_{T_n} \nabla_{xy} \cdot \vec{J}_h ds, \quad n = 1, \ldots, N1,$$

$$I_n^v = \int_{R_n} \frac{\partial}{\partial z} J_v ds, \quad n = N1, \ldots, N1 + N2 \tag{13}$$

where I_n is the nodal current of cell n; and $N1$ and $N2$ are the numbers of triangular and rectangular cells, respectively. The continuity equation provides the relationship between the surface charge densities and the surface current densities as

$$\sigma_h(\vec{r}) = -\frac{1}{j\omega} \vec{\nabla}_{xy} \cdot (\vec{J}_h + \vec{J}_h^e),$$

$$\sigma_v(\vec{r}) = -\frac{1}{j\omega} \frac{\partial}{\partial z} (J_v + J_v^e) \tag{14}$$

where $\vec{J}_h^e$ and J_v^e are the horizontal- and vertical-impressed current densities; and as defined previously, $\vec{J}_h$ and J_v are the horizontal- and vertical-induced current densities, respectively. As discussed before, excitations are treated as impressed current sources in circuit simulators. The inclusion of the impressed current densities in (14) provides the ability to do so. The continuity equation can also be described as

$$-j\omega \begin{bmatrix} \mathbf{Q}^h \\ \mathbf{Q}^v \end{bmatrix} = \begin{bmatrix} \mathbf{I}^h \\ \mathbf{I}^v \end{bmatrix} + \begin{bmatrix} \mathbf{I}^{eh} \\ \mathbf{I}^{ev} \end{bmatrix} \tag{15}$$

where Q_n, I_n, and I_n^e are the charge, the induced current, and the impressed current associated with cell n, respectively. The induced nodal currents are related to the induced branch-wise currents by the connectivity matrix as

$$\begin{bmatrix} \mathbf{I}^h \\ \mathbf{I}^v \end{bmatrix} = \begin{bmatrix} \mathbf{\Lambda}^T \end{bmatrix} \begin{bmatrix} \mathbf{i}^h \\ \mathbf{i}^v \end{bmatrix}. \tag{16}$$

As mentioned before, the surface charge density is constant over each cell (a property of the current basis functions). Thus, the charge density can be expressed using pulse basis functions as

$$\sigma(\vec{r}) = \sum_{n=1}^{N1+N2} \frac{Q_n}{A_n} p_n(\vec{r})$$

where

$$p_n(\vec{r}) = \begin{cases} 1, & \vec{r} \text{ in cell } n \\ 0, & \text{elsewhere} \end{cases}$$

is a pulse basis function, and A_n is the area of Cell n. Then, the surface electric potential is related to the surface charge density by the scalar electric potential Green's functions as

$$\phi(\vec{r}) = \int_{s1} \sigma_n(\vec{r}') G_x^\phi(\vec{r}, \vec{r}') ds'$$

$$+ \int_{s2} \sigma_v(\vec{r}') G_z^\phi(\vec{r}, \vec{r}') ds'$$

$$= \int_{s1} \sum_{n=1}^{N1} \frac{Q_n}{A_n} p_n(\vec{r}') G_x^\phi(\vec{r}, \vec{r}') ds'$$

$$+ \int_{s2} \sum_{n=N1+1}^{N1+N2} \frac{Q_n}{A_n} p_n(\vec{r}') G_z^\phi(\vec{r}, \vec{r}') ds'. \tag{17}$$

Equation (17) can be expressed in a matrix-equation notation as

$$\begin{bmatrix} \phi^h \\ \phi^v \end{bmatrix} = \begin{bmatrix} \mathbf{K}^{hh} & \mathbf{K}^{hv} \\ \mathbf{K}^{vh} & \mathbf{K}^{vv} \end{bmatrix} \begin{bmatrix} \mathbf{Q}^h \\ \mathbf{Q}^v \end{bmatrix} \tag{18}$$

where

$$K_{pq}^{hh} = \frac{1}{A_p A_q} \int_{T_p} \int_{T_q} G_x^\phi(\vec{r}, \vec{r}') ds' ds,$$

$$K_{pq}^{hv} = \frac{1}{A_p A_q} \int_{T_p} \int_{R_q} G_z^\phi(\vec{r}, \vec{r}') ds' ds,$$

$$K_{pq}^{vh} = \frac{1}{A_p A_q} \int_{R_p} \int_{T_q} G_x^\phi(\vec{r}, \vec{r}') ds' ds,$$

$$K_{pq}^{vv} = \frac{1}{A_p A_q} \int_{R_p} \int_{R_q} G_z^\phi(\vec{r}, \vec{r}') ds' ds. \tag{19}$$

From circuit theory, charge stored in a capacitor is the product of the voltage drop across the capacitor and its capacitance. Then the $\mathbf{K}$ matrix is the *inverse capacitance matrix*. It is cell-wise since ϕ and Q are both cell based. Then, using (9), (15), (16) and (18), a discretized form of a mixed-potential integral equation results as

$$\begin{bmatrix} j\omega \mathbf{C} & \mathbf{\Lambda}^T \\ -\mathbf{\Lambda} & j\omega \mathbf{L} \end{bmatrix} \begin{bmatrix} \phi \\ \mathbf{i} \end{bmatrix} = \begin{bmatrix} -\mathbf{I}^e \\ 0 \end{bmatrix} \tag{20}$$

where

$$[\mathbf{C}] = [\mathbf{K}]^{-1} = \begin{bmatrix} \mathbf{K}^{hh} & \mathbf{K}^{hv} \\ \mathbf{K}^{vh} & \mathbf{K}^{vv} \end{bmatrix}^{-1},$$

$$[\mathbf{L}] = \begin{bmatrix} \mathbf{L}^{hh} & 0 \\ \mathbf{L}^{vh} & \mathbf{L}^{vv} \end{bmatrix},$$

$$[\mathbf{i}] = \begin{bmatrix} \mathbf{i}^h \\ \mathbf{i}^v \end{bmatrix},$$

$$[\boldsymbol{\phi}] = \begin{bmatrix} \boldsymbol{\phi}^h \\ \boldsymbol{\phi}^v \end{bmatrix},$$

$$[\mathbf{I}^e] = \begin{bmatrix} \mathbf{I}^{eh} \\ \mathbf{I}^{ev} \end{bmatrix}. \tag{21}$$

This equation has a standard form of modified nodal analysis that is utilized in many circuit simulators [32]. The $\mathbf{L}$ matrix is asymmetric, as discussed before. The $\mathbf{C}$ matrix is also asymmetric, as shown in (19). Two different Green's functions G_x^ϕ and G_z^ϕ are used in the previous derivation. They represent the scalar-potential Green's functions for the point charge associated with an x- and a z-directed electric dipole. In a multilayer medium, the scalar potentials of point charges that are associated with a horizontal electric dipole (HED) and a vertical electric dipole (VED) are different [33]. Therefore, in general, the scalar-potential Green's function for the point charge that is associated with an arbitrarily oriented dipole doesn't exist in a stratified medium. However, in power bus structures, the surface currents are either horizontal or vertical, since the currents on the surfaces of vertical discontinuities are all assumed to be z-directional. So two different scalar-potential Green's functions, G_h^ϕ and G_v^ϕ, are specified and

$$G_h^\phi = G_x^\phi = G_y^\phi,$$
$$G_v^\phi = G_z^\phi \tag{22}$$

where G_y^ϕ is the scalar-potential Green's function for the point charge associated with a y-oriented electric dipole, and is the same as G_x^ϕ.

The currents at the intersection edges between vertical discontinuities and power plane must be continuous. In the previous formulations, two current densities are specified for every intersection edge, thus two unknown branch currents associated with one intersection edge are used in (20). To enforce current continuity, let these two unknowns be equal for every intersection edge. Then, the matrix equation becomes

$$\begin{bmatrix} j\omega\mathbf{C} & \boldsymbol{\Lambda}'^{\mathrm{T}} \\ -\boldsymbol{\Lambda}' & j\omega\mathbf{L}' \end{bmatrix} \begin{bmatrix} \boldsymbol{\phi} \\ \mathbf{i}' \end{bmatrix} = \begin{bmatrix} -\mathbf{I}^e \\ 0 \end{bmatrix} \tag{23}$$

where $\mathbf{L}'$, $\boldsymbol{\Lambda}'$, and $\mathbf{i}'$ are modified matrices or vectors, after the current continuity procedure is applied.

III. CIRCUIT EXTRACTION

There are two ways to extract an equivalent circuit model from (23), based on either loop currents or node potentials. If the equivalent circuit is extracted based on loop currents the mutual coupling terms, which may be in the forms of mutual inductances and current-controlled sources, which are hard to simulate in SPICE, will result. Therefore, the circuit extraction

used herein is based on node potentials. The extracted circuit includes $\mathbf{L}$ and $\mathbf{C}$ elements only. A pure relationship between the node potentials and the impressed node currents can be derived from (23), by back-substituting for the unknown $\mathbf{i}'$ vector, as

$$[\mathbf{Y}][\boldsymbol{\phi}] = [-\mathbf{I}^e] \tag{24}$$

where the $\mathbf{Y}$ matrix is denoted as the *nodal admittance matrix* of the system, and

$$[\mathbf{Y}] = \frac{1}{j\omega} \left[\boldsymbol{\Lambda}'^{\mathrm{T}} \mathbf{L}'^{-1} \boldsymbol{\Lambda}' \right] + j\omega[\mathbf{C}]. \tag{25}$$

As discussed before, the matrices $\mathbf{L}$ and $\mathbf{C}$ are asymmetric, and $\mathbf{L}'$ is also asymmetric. However, the complete field admittance matrix $\mathbf{Y}$ is symmetric, as the reciprocity theorem requires. Excitation can be specified in the right-hand $\mathbf{I}^e$ vector, and the corresponding node potentials can be obtained from (24).

Instead of directly solving (24), an equivalent circuit model is extracted from the admittance matrix. The prototype of the equivalent circuit used herein is the one with a circuit branch between every two circuit nodes (including every node to the common ground node). This circuit model will give good results, provided that the admittance matrix can be exactly restored for circuit simulations. At an arbitrary node m, according to (24), the nodal current is

$$I_m = \sum_n Y_{mn}\phi_n$$

$$= \sum_n Y_{mn}(\phi_n - \phi_m) + \left(\sum_n Y_{mn} \right)(\phi_m - 0) \tag{26}$$

where Y_{mn} is the entry at the mth row and the nth column in the admittance matrix, and ϕ_n is the potential of node n with respect to the ground node (here the ground plane). Note here that the Y_{mn} are elements of the inverse impedance matrix, and are from field quantities, namely, source-field reactions.

At the same time, for the circuit prototype described before, Kirchoff's current law (KCL) requires the balance of currents at every node, i.e.,

$$I_m = -\sum_{n \neq m} i_{n:m} + i_{m:0}$$

$$= -\sum_{n \neq m} Y_{m:n}(\phi_n - \phi_m) + Y_{m:0}(\phi_m - 0) \tag{27}$$

as shown in Fig. 4, where $m{:}n$ denotes a circuit branch connecting nodes m and n. $Y_{m:n}$ (a circuit quantity) is the admittance of this branch, and $i_{m:n}$ is the branch current. $Y_{m:0}$ is the admittance of the branch connecting node m to the common ground node. A comparison between (26) and (27) leads to

$$Y_{m:n} = -Y_{mn}, \quad m \neq n \text{ and } m \neq 0, \tag{28a}$$

$$Y_{m:0} = \sum_{n \neq m} Y_{mn} + Y_{mm}, \quad m \neq 0. \tag{28b}$$

From $Y_{m:n}$, the values of the equivalent circuit elements between nodes m and n can be directly determined. Since the $\mathbf{Y}$ matrix is the sum of an inductive part and a capacitive part, every branch (including node to ground) is a parallel LC circuit. The
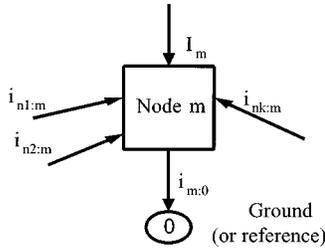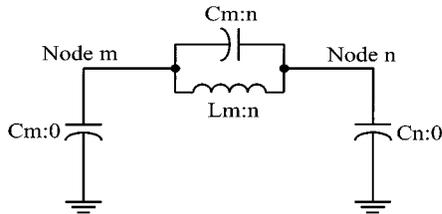
Fig. 4. Current balance at node m.

Fig. 5. Typical equivalent circuit between any arbitrary pair of two nodes m and n. For nodes with current flowing into ground plane, there is a shunt inductance as well.

values of L and C can be obtained through (28a) and (28b) from the inductive and capacitive parts of $\mathbf{Y}$ separately.

The entries in the $\mathbf{L}'$ and $\mathbf{C}$ matrices are functions of vector- or scalar-potential Green's functions, which are frequency dependent. Hence, the circuit that is extracted from (28a) and (28b) is also frequency dependent, which makes the circuit simulation difficult and time-consuming. A quasistatic approximation of the Green's functions is employed to overcome this problem. Then the values of extracted inductance and capacitance are constant over frequency. However, this approximation introduces an additional mesh constraint to keep the extracted circuit meaningful and valid for capturing the distributed behavior of the power bus up to a specified upper frequency. This limitation is determined by the highest frequency of interest, layer stackup, and dielectric materials [20].

Under the quasistatic approximation, it can be demonstrated that K_{pq}^{hv} is equal to K_{pq}^{vh}, *i.e.*, the matrix $\mathbf{C}$ is now symmetric. This results in asymmetry in the $\mathbf{Y}$ matrix, since the $\mathbf{L}'$ matrix is asymmetric. To restore the symmetry in $\mathbf{Y}$ (the circuit matrix whose entries are $Y_{m:n}$'s) that is required by circuit reciprocity, let [34]

$$L_{ij,\text{restored}}^{\prime hv} = L_{ji,\text{restored}}^{\prime vh} = \frac{L_{ij}^{\prime vh} + L_{ji}^{\prime vh}}{2}. \qquad (29)$$

The nondiagonal entries in the $\mathbf{L}'$ matrix are averaged so that the symmetry of the $\mathbf{L}'$ matrix, as well as of the $\mathbf{Y}$ matrix, is restored.

Fig. 5 shows a typical circuit between an arbitray pair of nodes m and n. A parallel LC branch exists between these two circuit nodes, and there is also a shunt capacitance between each node and the ground node. The shunt inductance to ground for the horizontal cells as indicated in (28b) is neglected, since its value is usually very large (There is no significant conduction current flowing into the ground plane.). However, for those nodes that are associated with cells that have vertical surface currents flowing into the ground plane, there is an inductance connecting from the node to the ground node as well. As shown
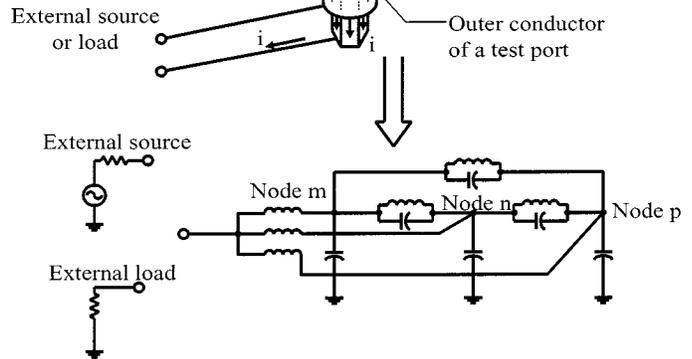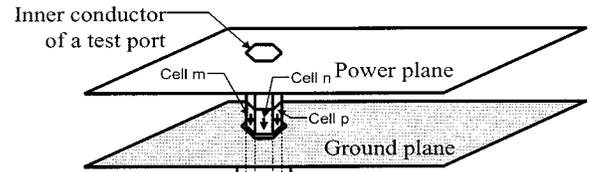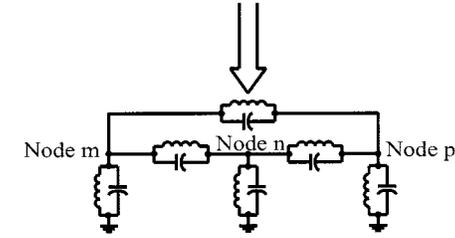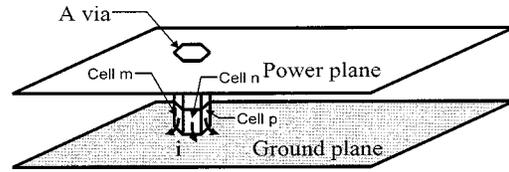

Fig. 6. Equivalent circuits for a via and a test port.

in Fig. 6, for a via connecting the power and ground planes, its vertical rectangular cells adjacent to the ground plane have surface currents flowing into the ground plane. The choice of the ground node is consistent with the choice of the Green's functions. Since all ground planes are assumed as infinitely large perfect electric conductors (PEC) and incorporated into the calculation of Green's functions, the resulting circuit refers to the ground planes as the ground node.

IV. CALCULATION OF GREEN'S FUNCTIONS

Calculation of the Green's functions for a multilayer structure involves the calculation of Sommerfeld integrals, which when evaluated using numerical techniques are very time-consuming. In order to accelerate the convergence of Sommerfeld integrals, many extrapolation methods have been developed. Michalski [35] gives an extensive review. In this work, the Green's functions are obtained using a different approach based on complex-image theory [36], [37], which is applied to the inverse Fourier transform from spectral to spatial domain based on the Sommerfeld identity. The spectral-domain expressions for the Green's functions are relatively straight-forward though tedious, to derive, since they are solutions to a one-dimensional (z-direction)

problem [38], assuming the dielectric layers and PEC ground plane are of infinite extent. The derivations and results are included in the Appendix.

The inverse Fourier transform is given by the Sommerfeld identity as [38]

$$\frac{e^{-jkr}}{4\pi r} = \frac{1}{4\pi}\int_{-\infty}^{\infty} k_\rho dk_\rho H_0^{(2)}(k_\rho \rho)\frac{e^{-jk_z|z|}}{2jk_z} \qquad (30)$$

i.e.,

$$\mathcal{F}^{-1}\left(\frac{e^{-jk_z|z|}}{2jk_z}\right) = \frac{e^{-jkr}}{4\pi r}. \qquad (31)$$

This identity is particularly useful in obtaining the spatial-domain Green's functions by approximating the spectral-domain expressions in a multilayer medium as a series of complex images

$$\tilde{G} = \frac{1}{2\gamma}\sum_{p=1}^{M}\alpha_p e^{\gamma a_p}, \qquad (32)$$

where

$$\gamma = jk_z.$$

Then, the spatial-domain expression can be obtained by substituting (32) into (30) and

$$G = \sum_{p=1}^{M}\alpha_p\frac{e^{-jk\sqrt{x^2+y^2+a_p^2}}}{4\pi\sqrt{x^2+y^2+a_P^2}}. \qquad (33)$$

Several numerical methods can be used to develop an approximate spectral-domain Green's function as a series of complex exponentials (complex images). The original Prony's method [36], and the least-square Prony's method [39], were first used. The efficiency and noise sensitivity problems associated with these Prony's methods were greatly improved by the generalized pencil of function (GPOF) method [40]. However, the GPOF method is not robust for slowly converging, rapidly varying functions. A further improvement to the GPOF method, denoted a two-level approach [37], is used in the CEMPIE modeling described in this work.

The dyadic vector potential Green's function for a multilayer medium has four components. As shown in the previous derivation, all four of these components, i.e., G_{zx}^A, G_{zy}^A, G_{xx}^A and G_{zz}^A, are required for the calculations of the moment matrix, since both horizontal and vertical current densities are present in the 3-D problem that includes vias. The evaluation of the components G_{zx}^A, G_{zy}^A and G_{zz}^A is considerably more complicated, as compared with the calculation of G_{xx}^A. When G_{xx}^A is calculated, the z-directional coordinates of all field and source points are fixed, since all horizontal electric dipoles are on one or more power planes. The spectral-domain expressions are the same for all the pairs of field and source locations with the same observation z and source z' coordinates. Then the inverse Fourier transform has to be performed only once. However, for the other three components, the z-directional coordinate of field point, or source point, or both, varies along the surfaces of vertical discontinuities. This means the spectral-domain expressions are different for the basis function pairs with different z and/or z'

coordinates; thus, the inverse Fourier transform must be performed for each of these pairs. The spectral-domain expressions are exponential functions that vary rapidly with z and z'. Therefore, even for a very small via, many spatial sample points are needed, which is very time consuming and impractical. The solution is to carry out the integration over z and/or z' analytically for the spectral domain expressions for the Green's function multiplied with the testing and/or basis function for each vertical cell [41]–[43]. Then the inverse Fourier transform needs only to be performed once for this vertical cell. When this procedure is applied, another problem arises. Commonly, the height of each vertical cell is not larger than 100 mils (2.54 mm). After the integration of the Green's function multiplied with the testing and/or basis function (which is a function of z or z'), the values obtained are too small to ensure that the GPOF procedure works properly with sufficient numerical precision. For this problem to be solved, the values of the GPOF input series must be scaled to an appropriate range, and then the GPOF output rescaled back.

Properly choosing the number of complex images that are used to approximate the spectral-domain expressions for the Green's functions is also critical. Effective approximations using complex images for the spectral-domain expressions for the Green's functions do not always ensure the correct spatial results, i.e., the generalized Sommerfeld identity does not apply for all the complex images resulting from the GPOF procedure. For example, the terms having very small coefficients and very large exponential indices are possible noise terms, which result in dramatic errors in far fields. Hence, these terms must be removed from the GPOF output. If these noise terms exist, a change in the number of complex images or in the criterion of determining noise is necessary. Further, the real part of the exponential index of each complex image should be greater than zero. Otherwise, the term will represent a convergent wave that cannot result from a real source. This feature provides another check for the GPOF output. If the real part of any exponential index is less than zero, the input parameters of the GPOF procedure should be adjusted and the method re-applied.

V. DC POWER BUS MODELING AND RESULTS

There are two kinds of vertical discontinuities of interest, *viz.*, via, and port types. As shown in Fig. 6, the via vertical discontinuity connects power and ground planes together, while the port vertical discontinuity (like an SMA connector) connects the inner conductor to a power plane and the outer conductor to a ground plane. For both types, there is a current associated with each intersection edge between the vertical discontinuities and the ground plane. This current flows across the edge, from the retangular cell associated with the edge (such as cells m, n and p in Fig. 6), and into the ground plane (for a via) or the external load/source (for a port). The connectivity matrix defined in (11) relates mesh edges (circuit branches) to mesh cells (circuit nodes). It can be shown by studying the basis functions that the current associated with an edge always flows from the edge's positive cell to its negative cell. Therefore, the rectangular cells adjacent to the ground plane (such as cells m, n, and p in Fig. 6) are positive cells of the corresponding intersection edges. The corresponding negative cells are the ground node (for a via), or
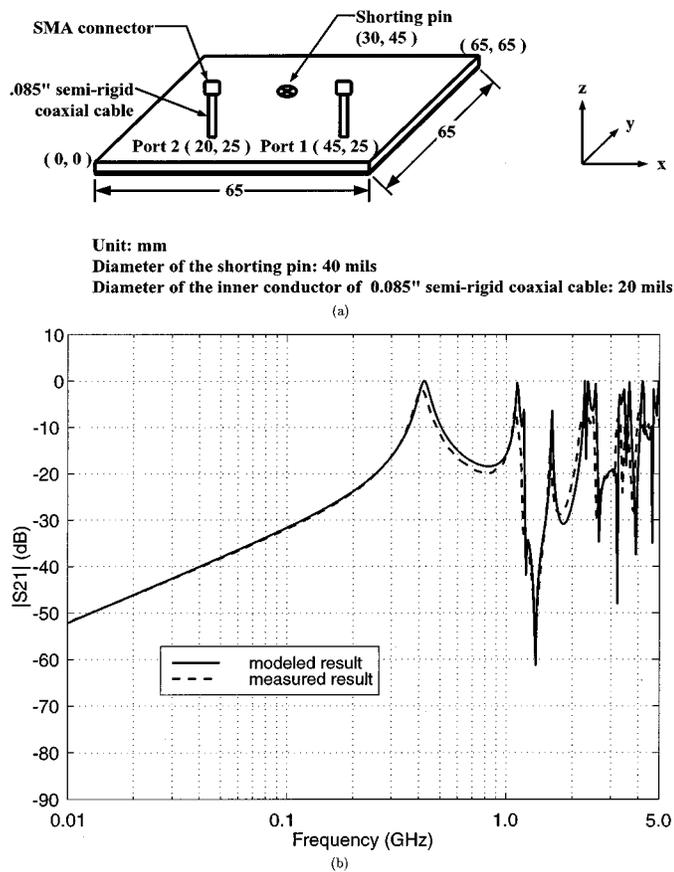
Fig. 7. Modeling a simple power bus geometry.

Fig. 8. Modeling a power island geometry.

an external node where an external load or source is connected (for a port). The connectivity matrix contains the information about the positive and negative cells of the intersection edges, thus, it determines whether the current flows into the ground plane or an external node. The equivalent circuits that are associated with the rectangular cells of a via, which are adjacent to the ground plane, will include an inductance connecting those cells (circuit nodes) to the ground node. However, for a port, the equivalent circuits that are associated with the rectangular cells adjacent to the ground plane will include an inductance connecting these cells to the external node, rather than the common ground node, where the external source or load is connected.

Several power-bus geometries were modeled with the CEMPIE approach, and compared with measurements. Fig. 7(a) shows a power-bus structure with a shorting post and two test ports. The test board was a two-layer board with two solid planes representing power and ground layers, respectively. The shorting post represented a via. The board was fabricated from FR-4 material, and the relative dielectric constant was $\varepsilon_r = 4.7$. The board thickness was 44 mils (1.12 mm), and the diameters of the via and the feed port conductor were 40 mils (1.02 mm) and 20 mils (0.508 mm), respectively. The $|S_{21}|$ between the two test ports was investigated experimentally using an HP8753D network analyzer. The reference planes were at the 3.5 mm test cable connectors. A simple 12-term error correction model using an open, short, and load was used in the calibration. Port extension was used to move the measurement plane to the coaxial cable feed terminals looking
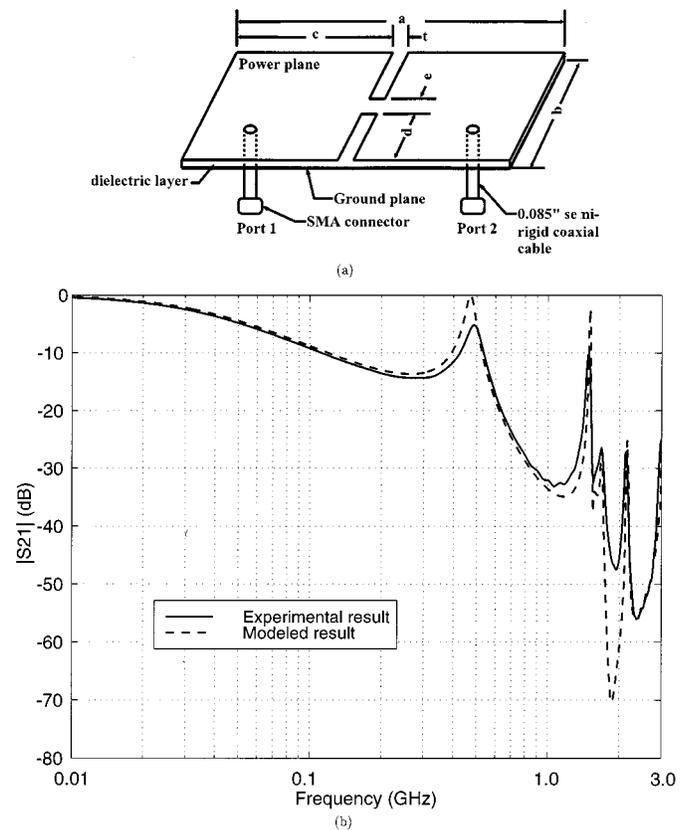
into the power bus. Fig. 7(b) shows the comparison between modeling and measurement. The results compare favorably up to 3 GHz. Beyond that, the modeled result predicts the correct trends. There are discrepancies in magnitude at resonances, but losses were not included in this model.

Another modeling example is a power-island geometry illustrated in Fig. 8(a). Results are shown in Fig. 8(b). The geometrical dimensions of the parameters in Fig. 8(a) used in the test board were $a = 100$ mm, $b = 55$ mm, $c = 49$ mm, $d = 25$ mm, $e = 5$ mm, and $t = 2$ mm. This test board also used an FR-4 material with the spacing between power and ground layers of 44 mils (1.12 mm). Again the measured and modeled results compare favorably, with discrepancies at the resonances dominated by the neglected losses in the CEMPIE modeling.

Fig. 9(a) illustrates a power bus geometry with an SMT decoupling capacitor. The dielectric layer material was FR-4 as well, with a relative dielectric constant of $\varepsilon_r = 4.7$, and loss tangent of 0.02. The PCB was 44 mils' (1.12 mm) thick and had two solid planes. A 0.1 μF SMT decoupling capacitor was placed on the board. One end of the capacitor was directly soldered to the ground plane, and the other end was connected to the power plane through a via. The input impedance at the test port was measured using an HP4291A impedance analyzer. The modeled results are compared with the measurements in Fig. 9(b). Good agreement is demonstrated up to 1.8 GHz, which is the maximum frequency of the impedance analyzer. The via and the test port were included in the first principles formulation, while the capacitor was incorporated into the CEMPIE extracted circuit model as a lumped series RLC circuit. The values of this
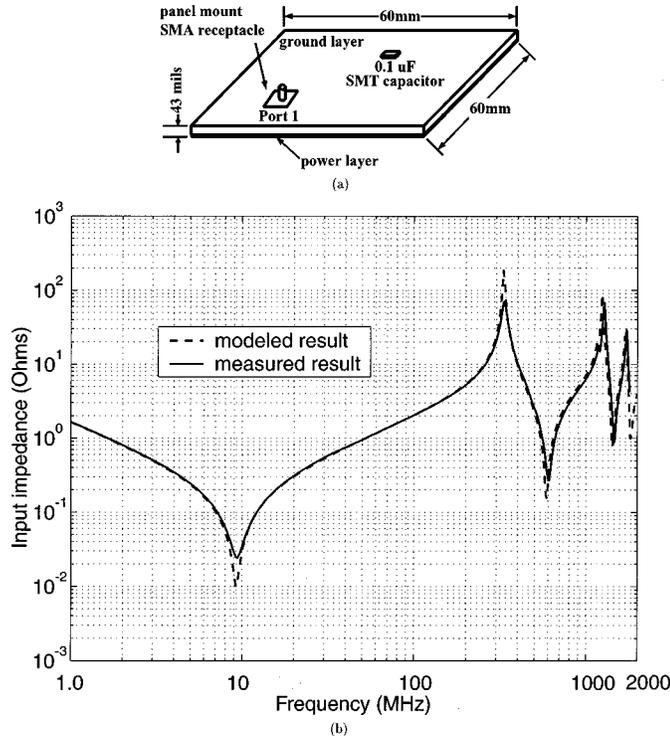
Fig. 9.   Modeling a power bus geometry with an SMT decoupling capacitor.

RLC circuit were measured using the impedance analyzer. In this modeling example, dielectric losses were included by using a complex dielectric constant.

VI. CONCLUSIONS

The CEMPIE formulation presented herein is derived from Maxwell's equations and uses a circuit extraction approach. The Green's functions for a stratified medium are used, instead of the free space Green's functions. Vertical discontinuities are included into the first principles formulation; hence, it is a 3D modeling approach which can deal with general power layer geometries. Measurements demonstrate that it is suitable for modeling multilayer PCB structures. With SPICE or IBIS models of IC components, and suitable transmission-line models for signals, CEMPIE can be used to model power-bus noise distributions and thus address SMT decoupling capacitor problems. Signal integrity (SI) and EMI design issues such as stackup configurations, gapped power layers, interplane capacitance, *etc.*, can also be addressed.

APPENDIX
SPECTRAL-DOMAIN EXPRESSIONS FOR GREENS'S FUNCTIONS

The spectral-domain Green's functions for a multilayer medium can be derived from the solution of one-dimensional problems. First, consider a case with a point source $\vec{J} = \hat{\alpha}\delta(\vec{r'})$ embedded in a homogeneous medium. The field solutions are

$$
\vec{E}(\vec{r}) = -j\omega\mu \left(\bar{\bar{I}} + \frac{\nabla\nabla}{k^2} \right) \cdot \hat{\alpha}\frac{e^{-jk|\vec{r}-\vec{r'}|}}{4\pi|\vec{r}-\vec{r'}|}
$$
$$
\vec{H}(\vec{r}) = \nabla \times \hat{\alpha}\frac{e^{-jk|\vec{r}-\vec{r'}|}}{4\pi|\vec{r}-\vec{r'}|}. \tag{34}
$$

For an horizontal electric dipole (HED), $\hat{\alpha} = \hat{x}$, then

$$
E_z = \frac{-j}{4\pi\omega\epsilon} \frac{\partial^2}{\partial z\partial x} \frac{e^{-jk|\vec{r}-\vec{r'}|}}{|\vec{r}-\vec{r'}|},
$$
$$
H_z = -\frac{1}{4\pi} \frac{\partial}{\partial y} \frac{e^{-jk|\vec{r}-\vec{r'}|}}{|\vec{r}-\vec{r'}|}. \tag{35}
$$

The Fourier transform is defined as

$$
\tilde{f}(k_x, k_y) = \int_{-\infty}^{\infty} dx e^{jk_x x} \int_{-\infty}^{\infty} dy e^{jk_y y} f(x, y), \tag{36}
$$

and the corresponding inverse transform as

$$
f(x, y) = \frac{1}{(2\pi)^2} \int_{-\infty}^{\infty} dk_x e^{-jk_x x} \int_{-\infty}^{\infty} dk_y y e^{-jk_y y} \tilde{f}(k_x, k_y)
$$
$$
= \frac{1}{4\pi} \int_{-\infty}^{\infty} dk_\rho k_\rho H_0^{(2)}(k_\rho\rho) \tilde{f}(k_\rho). \tag{37}
$$

Then, the spectral-domain expressions for E_z and H_z are

$$
\tilde{E}_z = \mp \frac{-k_\rho \cos\phi}{2\omega\epsilon} e^{[-jk_z|z-z'|]}
$$
$$
\tilde{H}_z = \frac{k_\rho \sin\phi}{2k_z} e^{[-jk_z|z-z'|]} \tag{38}
$$

where the negative sign is for $z > z'$, and the positive sign is for $z < z'$.

When the source is embedded in the multilayer medium shown in Fig. 10, the fields in the same layer as the source can be constructed from the solutions of the homogeneous case. The only modification is to include an upgoing wave and a downgoing wave into the z-variation of the solutions as

$$
\tilde{E}_{z,h}^{pp} = -\frac{k_x}{2\omega\epsilon_p}
$$
$$
\times \left[\mp e^{[-jk_{zp}|z-z'|]} \right.
$$
$$
\left. + B_h^e e^{jk_{zp}z} + D_h^e e^{-jk_{zp}z} \right]
$$
$$
\tilde{H}_{z,h}^{pp} = \frac{k_y}{2k_{zp}} \left[e^{[-jk_{zp}|z-z'|]} \right.
$$
$$
\left. + A_h^e e^{jk_{zp}z} + C_h^e e^{-jk_{zp}z} \right]. \tag{39}
$$

When boundary conditions are enforced at $z = h_{p-1}$

$$
B_h^e e^{jk_{zp}h_{p-1}} = \tilde{R}_{p+}^{TM} \left[-e^{[-jk_{zp}(h_{p-1}-z')]} \right.
$$
$$
\left. + D_h^e e^{[-jk_{zp}h_{p-1}]} \right]
$$
$$
A_h^e e^{jk_{zp}h_{p-1}} = \tilde{R}_{p+}^{TE} \left[e^{[-jk_{zp}(h_{p-1}-z')]} \right.
$$
$$
\left. + C_h^e e^{[-jk_{zp}h_{p-1}]} \right] \tag{40}
$$

and at $z = h_p$,

$$
D_h^e e^{-jk_{zp}h_p} = \tilde{R}_{p-}^{TM} \left[e^{[jk_{zp}(h_p-z')]} + B_h^e e^{jk_{zp}h_p} \right]
$$
$$
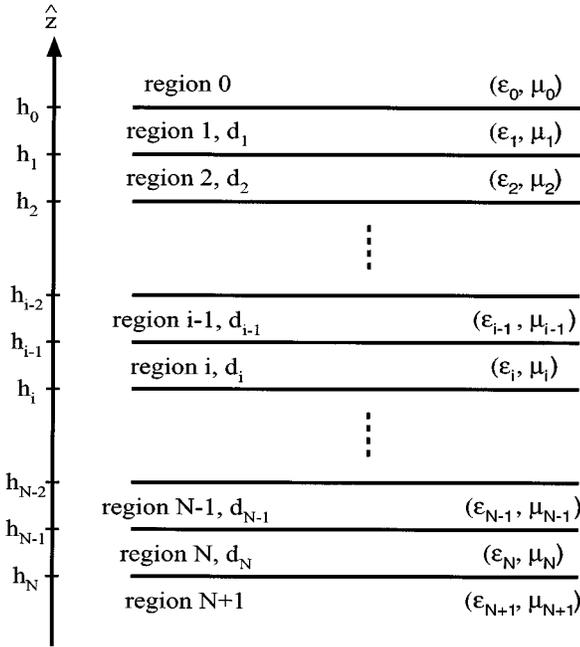C_h^e e^{-jk_{zp}h_p} = \tilde{R}_{p-}^{TE} \left[e^{[jk_{zp}(h_p-z')]} + A_h^e e^{jk_{zp}h_p} \right] \tag{41}
$$

Fig. 10.   Illustration of coordinates for a multilayer structure.

where $\tilde{R}^{\mathrm{TM}}$ and $\tilde{R}^{\mathrm{TE}}$ are Fresnel reflection coefficients [38], the unknown coefficients are then solved as

$$
\begin{aligned}
A_h^e =& e^{-\gamma_p h_{p-1}} \tilde{R}_{p+}^{\mathrm{TE}} \\
& \times \left[d^{[-\gamma_p(h_{p-1}-z')]} \right. \\
& \left. + \tilde{R}_{p-}^{\mathrm{TE}} \exp\left[\gamma_p(2h_p - h_{p-1} - z') \right] \right] \tilde{M}_p^{\mathrm{TE}}, \\
B_h^e =& e^{-\gamma_p h_{p-1}} \tilde{R}_{p+}^{\mathrm{TM}} \\
& \times \left[- e^{[-\gamma_p(h_{p-1}-z')]} \right. \\
& \left. + \tilde{R}_{p-}^{\mathrm{TM}} e^{[\gamma_p(2h_p - h_{p-1} - z')]} \right] \tilde{M}_p^{\mathrm{TM}} \\
C_h^e =& e^{\gamma_p h_p} \tilde{R}_{p-}^{\mathrm{TE}} \\
& \times \left[e^{\gamma_p(h_p - z')} \right. \\
& \left. + \tilde{R}_{p+}^{\mathrm{TE}} e^{[\gamma_p(h_p - 2h_{p-1}+z')]} \right] \tilde{M}_p^{\mathrm{TE}}, \\
D_h^e =& e^{\gamma_p h_p} \tilde{R}_{p-}^{\mathrm{TM}} \\
& \times \left[e^{\gamma_p(h_p - z')} \right. \\
& \left. - \tilde{R}_{p+}^{\mathrm{TM}} e^{[\gamma_p(h_p - 2h_{p-1}+z')]} \right] \tilde{M}_p^{\mathrm{TM}}
\end{aligned}
\tag{42}
$$

where

$$
\tilde{M}_p^{\mathrm{TE,TM}} = \left[1 - \tilde{R}_{p+}^{\mathrm{TE,TM}} \tilde{R}_{p-}^{\mathrm{TE,TM}} e^{-2\gamma_p d_p} \right]^{-1}.
$$

Further, the Green's functions are

$$
\tilde{G}_{xx}^{A(pp)} = \frac{\mu_p}{jk_y} \tilde{H}_{z,h}^{pp}
$$

$$
\tilde{G}_{zx}^{A(pp)} = \frac{k_p^2}{k_\rho^2} \left[\frac{1}{-j\omega} \tilde{E}_z^{pp} - \frac{k_x}{jk_p^2} \frac{\partial}{\partial z} \tilde{G}_{xx}^{A(pp)} \right]
$$

$$
\frac{j\omega}{k^2} \nabla \cdot \bar{\bar{G}}^A(\vec{r},\vec{r}') = \frac{1}{j\omega} \nabla' G^\phi(\vec{r},\vec{r}').
\tag{43}
$$

Substituting (39) and (42) into (43), the components of Green's functions are derived as

$$
\begin{aligned}
\tilde{G}_{xx}^{A(pp)} =& \frac{\mu_p}{2\gamma_p} \\
& \times \left\{ e^{[-\gamma_p|z-z'|]} + \tilde{M}_p^{\mathrm{TE}} \right. \\
& \times \left[\tilde{R}_{p+}^{\mathrm{TE}} e^{[-\gamma_p(2h_{p-1}-z-z')]} + \tilde{R}_{p-}^{\mathrm{TE}} \right. \\
& \times e^{[-\gamma_p(z+z'-2h_p)]} + \tilde{R}_{p+}^{\mathrm{TE}} \tilde{R}_{p-}^{\mathrm{TE}} \\
& \times \left(e^{[-\gamma_p(2d_p+z-z')]} \right. \\
& \left. \left. \left. + e^{[-\gamma_p(2d_p-z+z')]} \right) \right] \right\},
\end{aligned}
$$

$$
\begin{aligned}
\tilde{G}_{zx}^{A(pp)} =& \frac{\mu_p}{j2\gamma_p} \frac{k_x \gamma_\rho}{k_\rho^2} \\
& \times \left\{ \tilde{M}_p^{\mathrm{TM}} \left[-\tilde{R}_{p+}^{\mathrm{TM}} e^{[-\gamma_p(2h_{p-1}-z-z')]} \right. \right. \\
& + \tilde{R}_{p-}^{\mathrm{TM}} e^{[-\gamma_p(z+z'-2h_p)]} + \tilde{R}_{p+}^{\mathrm{TM}} \tilde{R}_{p-}^{\mathrm{TM}} \\
& \times \left(e^{[-\gamma_p(2d_p-z+z')]} \right. \\
& \left. \left. - e^{[-\gamma_p(2d_p+z-z')]} \right) \right] + \tilde{M}_p^{\mathrm{TE}} \\
& \times \left[-\tilde{R}_{p+}^{\mathrm{TE}} e^{[-\gamma_p(2h_{p-1}-z-z')]} \right. \\
& + \tilde{R}_{p-}^{\mathrm{TE}} e^{[-\gamma_p(z+z'-2h_p)]} + \tilde{R}_{p+}^{\mathrm{TE}} \tilde{R}_{p-}^{\mathrm{TE}} \\
& \times \left(e^{[-\gamma_p(2d_p+z-z')]} \right. \\
& \left. \left. \left. - e^{[-\gamma_p(2d_p-z+z')]} \right) \right] \right\}
\end{aligned}
$$

$$
\begin{aligned}
\tilde{G}_h^{\phi(pp)} =& \frac{1}{2\epsilon_p \gamma_p} \\
& \times \left\{ e^{[-\gamma_p|z-z'|]} + \tilde{M}_p^{\mathrm{TE}} \frac{\omega^2 \epsilon_p \mu_p}{\omega^2 \epsilon_p \mu_p + \gamma_p^2} \right. \\
& \times \left[\tilde{R}_{p+}^{\mathrm{TE}} e^{[-\gamma_p(2h_{p-1}-z-z')]} \right. \\
& + \tilde{R}_{p-}^{\mathrm{TE}} e^{[-\gamma_p(z+z'-2h_p)]} + \tilde{R}_{p+}^{\mathrm{TE}} \tilde{R}_{p-}^{\mathrm{TE}} \\
& \times \left(e^{[-\gamma_p(2d_p+z-z')]} \right. \\
& \left. \left. + e^{[-\gamma_p(2d_p-z+z')]} \right) \right] \\
& - \tilde{M}_p^{\mathrm{TM}} \frac{\gamma_p^2}{\omega^2 \epsilon_p \mu_p + \gamma_p^2} \\
& \times \left[\tilde{R}_{p+}^{\mathrm{TM}} e^{[-\gamma_p(2h_{p-1}-z-z')]} \right. \\
& + \tilde{R}_{p-}^{\mathrm{TM}} e^{[-\gamma_p(z+z'-2h_p)]} - \tilde{R}_{p+}^{\mathrm{TM}} \tilde{R}_{p-}^{\mathrm{TM}} \\
& \times \left(e^{[-\gamma_p(2d_p-z+z')]} \right. \\
& \left. \left. \left. + e^{[-\gamma_p(2d_p+z-z')]} \right) \right] \right\}.
\end{aligned}
\tag{44}
$$

Similar derivations from the field solutions of a vertical electric dipole (VED) give

$$\tilde{G}_{zz}^{A(pp)} = \frac{\mu_p}{2\gamma_p}$$
$$\times \left\{ e^{-\gamma_p|z-z'|} + \tilde{M}_p^{\mathrm{TM}} \right.$$
$$\times \left[\tilde{R}_{p+}^{\mathrm{TM}} e^{[-\gamma_p(2h_{p-1}-z-z')]} \right.$$
$$+ \tilde{R}_{p-}^{\mathrm{TM}} e^{[-\gamma_p(z+z'-2h_p)]}$$
$$+ \tilde{R}_{p+}^{\mathrm{TM}} \tilde{R}_{p-}^{\mathrm{TM}} \left(e^{[-\gamma_p(2d_p-z+z')]} \right.$$
$$\left. \left. \left. + e^{[-\gamma_p(2d_p+z-z')]} \right) \right] \right\},$$

$$\tilde{G}_v^{\phi(pp)} = \frac{1}{2\epsilon_p\gamma_p}$$
$$\times \left\{ e^{-\gamma_p|z-z'|} + \tilde{M}_p^{\mathrm{TM}} \right.$$
$$\times \left[-\tilde{R}_{p+}^{\mathrm{TM}} e^{[-\gamma_p(2h_{p-1}-z-z')]} \right.$$
$$- \tilde{R}_{p-}^{\mathrm{TM}} e^{[-\gamma_p(z+z'-2h_p)]}$$
$$+ \tilde{R}_{p+}^{\mathrm{TM}} \tilde{R}_{p-}^{\mathrm{TM}} \left(e^{[-\gamma_p(2d_p-z+z')]} \right.$$
$$\left. \left. \left. + e^{[-\gamma_p(2d_p+z-z')]} \right) \right] \right\}. \tag{45}$$

When field and source points are in different layers, the derivation of the spectral-domain expressions for the Green's functions needs to apply the concept of generalized transmission coefficient [38]. If the field and source points are in layers i and p, respectively, where $i < p$, then the field solutions in layer i for an HED embedded in layer p can be written as

$$\tilde{E}_{z,h}^{ip} = A_i^{\mathrm{TM}+} \left[e^{-\gamma_i z} + \tilde{R}_{i+}^{\mathrm{TM}} e^{[\gamma_i(z-2h_{i-1})]} \right]$$
$$\tilde{H}_{z,h}^{ip} = A_i^{\mathrm{TE}+} \left[e^{-\gamma_i z} + \tilde{R}_{i+}^{\mathrm{TE}} e^{[\gamma_i(z-2h_{i-1})]} \right]$$
$$\tag{46}$$

where $A_i^{\mathrm{TM}+}$ and $A_i^{\mathrm{TE}+}$ are coefficients of upgoing wave components in $\tilde{E}_{z,h}^{ip}$ and $\tilde{H}_{z,h}^{ip}$, respectively. From previous solutions, at $z = h_{p-1}$,

$$A_p^{\mathrm{TM}+} = -\frac{k_x}{2\omega\epsilon_p} \left[-e^{\gamma_p z'} + \tilde{R}_{P-}^{\mathrm{TM}} e^{[-\gamma_p(z'-2h_p)]} \right]$$
$$\times \tilde{M}_p^{\mathrm{TM}} e^{-\gamma_p h_{p-1}},$$
$$A_p^{\mathrm{TE}+} = -\frac{k_y}{j2\gamma_p} \left[e^{\gamma_p z'} + \tilde{R}_{P-}^{\mathrm{TE}} e^{[-\gamma_p(z'-2h_p)]} \right]$$
$$\times \tilde{M}_p^{\mathrm{TE}} e^{-\gamma_p h_{p-1}}. \tag{47}$$

When boundary conditions are enforced at $z = h_i$

$$A_i^+ e^{-\gamma_i h_i} = \tilde{T}_{pi} A_p^+ + \tilde{R}_{i-} A_i^+ e^{[\gamma_i(h_i-2h_{i-1})]} \tag{48}$$

a simple relationship between A_i^+ and A_p^+ (for both TM and TE cases) results

$$A_i^+ = e^{\gamma_i h_i} \tilde{T}_{pi} \tilde{M}_i A_p^+. \tag{49}$$

Once $A_i^{\mathrm{TM}+}$ and $A_i^{\mathrm{TE}+}$ are solved, the following components of Green's functions can be calculated from $\tilde{E}_{z,h}^{ip}$ and $\tilde{H}_{z,h}^{ip}$

$$\tilde{G}_{xx}^{A(ip)} = \frac{\mu_i}{2\gamma_p} \tilde{T}_{pi}^{\mathrm{TE}} \tilde{M}_p^{\mathrm{TE}} \tilde{M}_i^{\mathrm{TE}}$$
$$\times \left[e^{[-\gamma_i(z-h_i)]} \right.$$
$$\left. + \tilde{R}_{i+}^{\mathrm{TE}} e^{[-\gamma_i(2h_{i-1}-h_i-z)]} \right]$$
$$\times \left[e^{[-\gamma_p(h_{p-1}-z')]} \right.$$
$$\left. + \tilde{R}_{p-}^{\mathrm{TE}} e^{[-\gamma_p(z'+h_{p-1}-2h_p)]} \right],$$

$$\tilde{G}_{zx}^{A(ip)} = \frac{\mu_p}{j2\gamma_p} \frac{k_x}{\omega^2\epsilon_p\mu_p+\gamma_p^2}$$
$$\times \left\{ \gamma_p \tilde{T}_{pi}^{\mathrm{TM}} \tilde{M}_p^{\mathrm{TM}} \tilde{M}_i^{\mathrm{TM}} \right.$$
$$\times \left[e^{[-\gamma_i(z-h_i)]} \right.$$
$$\left. + \tilde{R}_{i+}^{\mathrm{TM}} e^{[-\gamma_i(2h_{i-1}-h_i-z)]} \right]$$
$$\times \left[-e^{[-\gamma_p(h_{p-1}-z')]} \right.$$
$$\left. + \tilde{R}_{p-}^{\mathrm{TM}} e^{[-\gamma_p(z'+h_{p-1}-2h_p)]} \right]$$
$$- \gamma_i \tilde{T}_{pi}^{\mathrm{TE}} \tilde{M}_p^{\mathrm{TE}} \tilde{M}_i^{\mathrm{TE}} \frac{\mu_i}{\mu_p}$$
$$\times \left[-e^{[-\gamma_i(z-h_i)]} \right.$$
$$\left. + \tilde{R}_{i+}^{\mathrm{TE}} e^{[-\gamma_i(2h_{i-1}-h_i-z)]} \right]$$
$$\times \left[e^{[-\gamma_p(h_{p-1}-z')]} \right.$$
$$\left. \left. + \tilde{R}_{p-}^{\mathrm{TE}} e^{[-\gamma_p(z'+h_{p-1}-2h_p)]} \right] \right\},$$

$$\tilde{G}_h^{\phi(ip)} = \frac{1}{2\gamma_p\epsilon_p} \frac{1}{\omega^2\epsilon_i\mu_i+\gamma_i^2}$$
$$\times \left\{ \frac{\omega^2\epsilon_i\mu_i^2}{\mu_p} \tilde{T}_{pi}^{\mathrm{TE}} \tilde{M}_p^{\mathrm{TE}} \tilde{M}_i^{\mathrm{TE}} \right.$$
$$\times \left[e^{[-\gamma_i(z-h_i)]} \right.$$
$$\left. + \tilde{R}_{i+}^{\mathrm{TE}} e^{[-\gamma_i(2h_{i-1}-h_i-z)]} \right]$$
$$\times \left[e^{[-\gamma_p(h_{p-1}-z')]} \right.$$
$$\left. + \tilde{R}_{p-}^{\mathrm{TE}} e^{[-\gamma_p(z'+h_{p-1}-2h_p)]} \right]$$
$$+ \gamma_i\gamma_p \tilde{T}_{pi}^{\mathrm{TM}} \tilde{M}_p^{\mathrm{TM}} \tilde{M}_i^{\mathrm{TM}}$$
$$\times \left[-e^{[-\gamma_i(z-h_i)]} \right.$$
$$\left. + \tilde{R}_{i+}^{\mathrm{TM}} e^{[-\gamma_i(2h_{i-1}-h_i-z)]} \right]$$
$$\times \left[-e^{[-\gamma_p(h_{p-1}-z')]} \right.$$
$$\left. \left. + \tilde{R}_{p-}^{\mathrm{TM}} e^{[-\gamma_p(z'+h_{p-1}-2h_p)]} \right] \right\}. \tag{50}$$

Similar derivations from the field solutions in layer i of a VED that is embedded in layer p, where $i < p$, give

$$\tilde{G}_{zz}^{A(ip)} = \frac{\mu_p}{2\gamma_p}\tilde{T}_{pi}^{\mathrm{TM}}\tilde{M}_i^{\mathrm{TM}}\tilde{M}_p^{\mathrm{TM}}$$
$$\times \left[e^{[-\gamma_p(h_{p-1}-z')]}\right.$$
$$\left. + \tilde{R}_{p-}^{\mathrm{TM}}e^{[-\gamma_p(h_{p-1}+z'-2h_p)]}\right]$$
$$\times \left[e^{-\gamma_i(z-h_i)}\right.$$
$$\left. + \tilde{R}_{i+}^{\mathrm{TM}}e^{[-\gamma_i(2h_{i-1}-z-h_i)]}\right]$$

$$\tilde{G}_v^{\phi(ip)} = -\frac{1}{2\epsilon_p\gamma_p}\frac{\gamma_i}{\gamma_p}\tilde{T}_{pi}^{\mathrm{TM}}\tilde{M}_i^{\mathrm{TM}}\tilde{M}_p^{\mathrm{TM}}$$
$$\times \left[e^{[-\gamma_p(h_{p-1}-z')]}\right.$$
$$\left. - \tilde{R}_{p-}^{\mathrm{TM}}e^{[-\gamma_p(h_{p-1}+z'-2h_p)]}\right]$$
$$\times \left[-e^{[-\gamma_i(z-h_i)]}\right.$$
$$\left. + \tilde{R}_{i+}^{\mathrm{TM}}e^{[-\gamma_i(2h_{i-1}-z-h_i)]}\right]. \qquad (51)$$

When the field point is in layer j, where $j > p$ and p is the source layer, the components of Green's functions are

$$\tilde{G}_{xx}^{A(jp)} = \frac{\mu_j}{2\gamma_p}\tilde{T}_{pj}^{\mathrm{TE}}\tilde{M}_p^{\mathrm{TE}}\tilde{M}_j^{\mathrm{TE}}$$
$$\times \left[e^{[-\gamma_j(h_{j-1}-z)]}\right.$$
$$\left. + \tilde{R}_{j-}^{\mathrm{TE}}e^{[-\gamma_j(h_{j-1}+z-2h_j)]}\right]$$
$$\times \left[e^{[-\gamma_p(z'-h_p)]}\right.$$
$$\left. + \tilde{R}_{p+}^{\mathrm{TE}}e^{[-\gamma_p(2h_{p-1}-z'-h_p)]}\right]$$

$$\tilde{G}_{zx}^{A(jp)} = \frac{\mu_p}{j2\gamma_p}\frac{k_x}{\omega^2\epsilon_p\mu_p+\gamma_p^2}$$
$$\times \left\{\gamma_p\tilde{T}_{pj}^{\mathrm{TM}}\tilde{M}_p^{\mathrm{TM}}\tilde{M}_j^{\mathrm{TM}}\right.$$
$$\times \left[e^{[-\gamma_j(h_{j-1}-z)]}\right.$$
$$\left. + \tilde{R}_{j-}^{\mathrm{TM}}e^{[-\gamma_j(h_{j-1}+z-2h_j)]}\right]$$
$$\times \left[e^{[-\gamma_p(z'-h_p)]}\right.$$
$$\left. - \tilde{R}_{p+}^{\mathrm{TM}}e^{[-\gamma_p(2h_{p-1}-z'-h_p)]}\right]$$
$$- \gamma_j\tilde{T}_{pj}^{\mathrm{TE}}\tilde{M}_p^{\mathrm{TE}}\tilde{M}_j^{\mathrm{TE}}\frac{\mu_j}{\mu_p}$$
$$\times \left[e^{[-\gamma_j(h_{j-1}-z)]}\right.$$
$$\left. - \tilde{R}_{j-}^{\mathrm{TE}}e^{[-\gamma_j(h_{j-1}+z-2h_j)]}\right]$$
$$\times \left[e^{[-\gamma_p(z'-h_p)]}\right.$$
$$\left. + \tilde{R}_{p+}^{\mathrm{TE}}e^{[-\gamma_p(2h_{p-1}-z'-h_p)]}\right]\right\},$$

$$\tilde{G}_h^{\phi(jp)} = \frac{1}{2\gamma_p\epsilon_p}\frac{1}{\omega^2\epsilon_j\mu_j+\gamma_j^2}$$
$$\times \left\{\frac{\omega^2\epsilon_j\mu_j^2}{\mu_p}\tilde{T}_{pj}^{\mathrm{TE}}\tilde{M}_p^{\mathrm{TE}}\tilde{M}_j^{\mathrm{TE}}\right.$$

$$\times \left[e^{[-\gamma_j(h_{j-1}-z)]}\right.$$
$$\left. + \tilde{R}_{j-}^{\mathrm{TE}}e^{[-\gamma_j(h_{j-1}+z-2h_j)]}\right]$$
$$\times \left[e^{[-\gamma_p(z'-h_p)]}\right.$$
$$\left. + \tilde{R}_{p+}^{\mathrm{TE}}e^{[-\gamma_p(2h_{p-1}-z'-h_p)]}\right]$$
$$+ \gamma_j\gamma_p\tilde{T}_{pj}^{\mathrm{TM}}\tilde{M}_p^{\mathrm{TM}}\tilde{M}_j^{\mathrm{TM}}$$
$$\times \left[e^{[-\gamma_j(h_{j-1}-z)]}\right.$$
$$\left. - \tilde{R}_{j-}^{\mathrm{TM}}e^{[-\gamma_j(h_{j-1}+z-2h_j)]}\right]$$
$$\times \left[e^{[-\gamma_p(z'-h_p)]}\right.$$
$$\left. - \tilde{R}_{p+}^{\mathrm{TM}}e^{[-\gamma_p(2h_{p-1}-z'-h_p)]}\right]\right\},$$

$$\tilde{G}_{zz}^{A(jp)} = \frac{\mu_p}{2\gamma_p}\tilde{T}_{pj}^{\mathrm{TM}}\tilde{M}_j^{\mathrm{TM}}\tilde{M}_p^{\mathrm{TM}}$$
$$\times \left[e^{[-\gamma_p(z'-h_p)]}\right.$$
$$\left. + \tilde{R}_{p+}^{\mathrm{TM}}e^{[-\gamma_p(2h_{p-1}-z'-h_p)]}\right]$$
$$\times \left[e^{[-\gamma_j(h_{j-1}-z)]}\right.$$
$$\left. + \tilde{R}_{j-}^{\mathrm{TM}}e^{[-\gamma_j(h_{j-1}+z-2h_j)]}\right]$$

$$\tilde{G}_v^{\phi(jp)} = -\frac{1}{2\epsilon_p\gamma_p}\frac{\gamma_j}{\gamma_p}\tilde{T}_{pj}^{\mathrm{TM}}\tilde{M}_j^{\mathrm{TM}}\tilde{M}_p^{\mathrm{TM}}$$
$$\times \left[-e^{[-\gamma_p(z'-h_p)]}\right.$$
$$\left. + \tilde{R}_{p+}^{\mathrm{TM}}e^{[-\gamma_p(2h_{p-1}-z'-h_p)]}\right]$$
$$\times \left[e^{[-\gamma_j(h_{j-1}-z)]}\right.$$
$$\left. - \tilde{R}_{j-}^{\mathrm{TM}}e^{[-\gamma_j(h_{j-1}+z-2h_j)]}\right]. \qquad (52)$$

REFERENCES

[1] R. Senthinathan and J. L. Prince, *Simultaneous Switching Noise of CMOS Devices and Systems*. Boston, MA: Kluwer, 1994.

[2] H. W. Johnson and M. Graham, *High-Speed Digital Design, a Handbook of Black Magic*. Englewood Cliffs, NJ: Prentice Hall, 1993.

[3] C. R. Paul, *Introduction to Electromagnetic Compatibility*. New York: Wiley, 1992.

[4] G. L. Ginsberg, *Printed Circuits Design*. New York: McGraw Hill, 1991.

[5] T. H. Hubing, J. L. Drewniak, T. P. Van Doren, and D. Hockanson, "Power bus decoupling on multilayer printed circuit boards," *IEEE Trans. Electromagn. Compat.*, vol. 37, pp. 155–166, May 1995.

[6] L. D. Smith, "Decoupling capacitor calculations for CMOS circuits," in *Proc. Elect. Perform. Elect. Packag. Conf.*, Monterey, CA, Nov. 2–4, 1994, pp. 101–105.

[7] A. R. Djordjevic and T. K. Sarkar, "An investigation of delta-I noise on integrated circuits," *IEEE Trans. Electromagn. Compat.*, vol. 35, pp. 134–147, May 1993.

[8] J. Fang, Y. Liu, Y. Chen, Z. Wu, and A. Agrawal, "Modeling of power/ground plane noise in high speed digital electronics packaging," in *Proc. IEEE 2nd Topical Meeting Elect. Perform. Electron. Packag.*, Monterey, CA, Oct. 1993, pp. 206–208.

[9] J. C. Parker, "Via coupling within parallel rectangular planes," *IEEE Trans. Electromagn. Compat.*, vol. 39, pp. 17–23, Feb. 1997.

[10] G. T. Lei, R. W. Techentin, P. R. Hayes, D. J. Schwab, and B. K. Gilbert, "Wave model solution to the ground/power plane noise problem," *IEEE Trans. Instrum. Meas.*, vol. 44, pp. 300–303, Apr. 1995.

[11] G. T. Lei, R. W. Techentin, and B. K. Gilbert, "High-frequency characterization of power/ground-plane structures," *IEEE Trans. Microwave Theory Tech.*, vol. 47, pp. 562–569, May 1999.

[12] W. D. Beckaer and R. Mittra, "FDTD modeling of noise in computer packages," in *Proc. 1993 IEEE Multichip Module Conf.*, Santa Clara, CA, March 15–18, 1993, pp. 123–127.

[13] X. D. Cai, G. L. Costache, R. Laroussi, and R. Crawhall, "Numerical extraction of partial inductance of package reference (power/ground) planes," in *Proc. IEEE Int. Symp. Electromagn. Compat.*, 1995, pp. 12–15.

[14] A. E. Ruehli, "Equivalent circuit models for three-dimensional multiconductor systems," *IEEE Trans. Microwave Theory Tech.*, vol. MTT-22, pp. 216–221, Mar. 1974.

[15] A. E. Ruehli and H. Heeb, "Circuit models for three-dimensional geometrices including dielectrics," *IEEE Trans. Microwave Theory Tech.*, vol. 40, pp. 1507–1515, July 1992.

[16] B. Archambeault and A. Ruehli, "Electrical package modeling including voltage and ground reference planes using the Partial Element Equivalent Circuit (PEEC) method," in *Proc. 13th Int. Zurich Symp. Tech. Exhibition Electromagn. Compat.*, Feb. 1999, pp. 233–238.

[17] P. Johns and R. Beurle, "Numerical solution of 2-d scattering problem using transmission line matrix," *Proc. IEEE*, vol. 59, pp. 1203–1208, Sept. 1971.

[18] J. G. Yook, V. Chandramouli, L. P. B. Katehi, K. A. Sakallah, T. R. Arabi, and T. A. Schreyer, "Computation of switching noise in printed circuit boards," *IEEE Trans. Comp., Packag., Manufact. Technol. A*, vol. 20, pp. 64–75, Mar. 1997.

[19] K. Lee and A. Barber, "Modeling and analysis of multichip module power supply planes," *IEEE Trans. Comp., Packag., Manufact. Technol. B*, vol. 18, pp. 628–639, Nov. 1995.

[20] H. Shi, "Study of printed circuit board power-bus design with a circuit extraction technique based on a quasi-static MPIE/MOM formulation," Ph.D. thesis, Dept. Elect. Comput. Eng., Univ. of Missouri-Rolla, 1997.

[21] J. Fan, "Modeling and design of dc power buses in high-speed digital circuit designs," Ph.D. thesis, Dept. Elect. Comput. Eng., Univ. Missouri-Rolla, 2000.

[22] T. H. Hubing, T. P. Van Doren, F. Sha, J. L. Drewniak, and M. J. Wilhem, "An experimental investigation of 4-layer printed circuit board decoupling," in *Proc. IEEE Int. Symp. Electromagn. Compat.*, Aug. 1995, pp. 308–312.

[23] H. Shi, F. Sha, J. L. Drewniak, T. P. Van Doren, and T. H. Hubing, "An experimental procedure for characterizing interconnects to the dc power bus on a multi-layer printed circuit board," *IEEE Trans. Electromagn. Compat.*, vol. 39, pp. 279–285, Nov. 1997.

[24] J. Fan, H. Shi, J. L. Drewniak, T. H. Hubing, R. E. DuBroff, and T. P. Van Doren, "Incorporating vertical discontinuities in power-bus modeling using a mixed-potential integral equation and circuit extraction formulation," in *Proc. 7th Topical Meeting Elect. Perform. Electron. Packag.*, West Point, NY, Oct. 26–28, 1998.

[25] S. M. Rao, D. R. Wilton, and A. W. Glisson, "Electromagnetic scattering by surfaces of arbitrary shape," *IEEE Trans. Antennas Propagat.*, vol. AP-30, pp. 409–418, May 1982.

[26] G. Dural and M. I. Aksun, "Closed-form Green's functions for general sources and stratified media," *IEEE Trans. Microwave Theory Tech.*, vol. 43, pp. 1545–1552, July 1995.

[27] R. F. Harrington, *Time-Harmonic Electromagnetic Fields*.   New York: McGraw-Hill., 1961.

[28] J. A. Kong, *Electromagnetic Wave Theory*, 2nd ed.   New York: Wiley, 1990.

[29] F. Y. Yuan, T. K. Postel, and L. M. Rubin, "Analysis and modeling of power distribution networks and plane structures in multichip modules and PCBs," in *Proc. IEEE Int. Symp. Electromagn. Compat.*, 1995, pp. 447–452.

[30] A. Sommerfeld, *Partial Differential Equations*.   New York: Academic, 1949.

[31] A. Banos, *Dipole Radiation in the Presence of a Conducting Half-Space*.   New York: Pergamon, 1969.

[32] C. W. Ho, A. E. Ruehli, and P. A. Brennan, "The modified nodal approach to network analysis," *IEEE Trans. Circuits Syst.*, vol. CAS-22, pp. 504–509, June 1975.

[33] K. A. Michalski, "On the scalar potential of a point charge associated with a time-harmonic dipole in a layered medium," *IEEE Trans. Antennas Propagat.*, vol. AP-35, pp. 1299–1301, Nov. 1987.

[34] C. H. Chan and R. A. Kipp, "Application of the complex image method to characterization of microstrip vias," *Int. J. Microwave Millim.-wave CAE*, vol. 7, pp. 368–379, 1997.

[35] K. A. Michalski, "Extrapolation methods for Sommerfeld Integral Tails," *IEEE Trans. Antennas Propagat.*, vol. 46, pp. 1405–1418, Oct. 1998.

[36] Y. L. Chow, J. J. Yang, D. G. Fang, and G. E. Howard, "A closed-form spatial Green's function for the thick microstrip substrate," *IEEE Trans. Microwave Theory Tech.*, vol. 39, pp. 588–592, Mar. 1991.

[37] M. I. Aksun, "A robust approach for the derivation of closed-form Green's functions," *IEEE Trans. Microwave Theory Tech.*, vol. 44, pp. 651–658, May 1996.

[38] W. C. Chew, *Waves and Fields in Inhomogeneous Media*.   Piscataway, New Jersey: IEEE Press, 1995.

[39] R. M. Shubair and Y. L. Chow, "Efficient computation of periodic Green's function in layered dielectric media," *IEEE Trans. Microwave Theory Tech.*, vol. 41, pp. 498–502, Mar. 1993.

[40] T. K. Sarkar and O. Pereira, "Using the matrix pencil method to estimate the parameters of a sum of complex exponentials," *IEEE Antennas Propagat. Mag.*, vol. 37, pp. 48–55, Feb. 1995.

[41] K. A. Michalski and D. Zhang, "Electromagnetic scattering and radiation by surfaces of arbitrary shape in layered media, Part I: Theory," *IEEE Trans. Antennas Propagat.*, vol. 38, pp. 335–344, Mar. 1990.

[42] M. I. Aksun and R. Mittra, "Efficient use of closed-form Green's functions for three-dimensional problems involving multilayered media," in *Proc. IEEE Antennas Propagat. Soc. Int. Symp.*, vol. 2, June 1994, pp. 1354–1357.

[43] N. Kinayman and M. I. Aksun, "Efficient use of closed-form Green's functions for the analysis of planar geometries with vertical connections," *IEEE Trans. Microwave Theory Tech.*, vol. 45, pp. 593–603, May 1997.

Jun Fan (S'97–M'00) received the B.S. and M.S. degrees in electrical engineering from Tsinghua University, Beijing, China, in 1994 and 1997, respectively, and the Ph.D. degree in electrical engineering from the University of Missouri-Rolla in 2000.

He is with NCR Corporation, San Diego, CA, where he is a Senior Hardware Engineer. His research interests include signal integrity and EMI designs in high-speed digital systems, dc power bus modeling, PCB noise reduction, and differential signaling.

Dr. Fan received the Conference Best Paper Award from the Applied Computational Electromagnetics Society in 2000.

Hao Shi (S'93–M'98) received the B.Sc. degree in microelectronic from Beijing University, Beijing, China, in 1984 and the M.S. and Ph.D. degrees in electrical engineering from the Electromagnetic Compatibility Laboratory, University of Missouri-Rolla, in 1995 and 1997, respectively.

He has been with Agilent Technologies, Santa Rosa, CA, as a Software Design Engineer since 1996. His professional interests include modeling of signal integrity in printed circuit boards, simulation of discontinuities in RF/microwave devices, and error analysis in lightwave communication systems.

Dr. Shi received the President's Memorial Award from the IEEE-EMC Society in 1995.

Antonio Orlandi (M'90–SM'97) was born in Milan, Italy in 1963. He received the Laurea degree in electrical engineering from the University of Rome "La Sapienza," Italy, in 1988.

He was with the Department of electrical Engineering, University of Rome "La Sapienza," from 1988 to 1990. In 1990, he was appointed Assistant Professor, and in 1998, Associate Professor with the Department of Electrical Engineering, University of L'Aquila, Italy. He has published papers in the field of electromagnetic compatibility in lightning protection systems and power drive systems. Current research interests are in the field of numerical methods to approach signal integrity issues in high speed digital systems.

Dr. Orlandi received the IEEE TRANSACTIONS ON ELECTROMAGNETIC COMPATIBILITY Best Paper Award in 1997. He is member of the Education and TC-9 Computational Electromagnetics Committees of the IEEE EMC Society, the editorial boards of the *Applied Computational Electromagnetic Society* (ACES) *Journal* and Chairman of the "EMC INNOVATION" Technical Committee of the International Zurich Symbosium and Technical Exhibition of EMC.

James L. Knighten (S'62–M'77–SM'97) received the B.S. and M.S. degrees in electrical engineering from Louisiana State University, Baton Rouge, in 1965 and 1968, respectively, and the Ph.D. degree in electrical engineering from Iowa State University, Ames, in 1976.

He is with NCR Corporation, San Diego, CA, and serves as a Technical Consultant. Since 1996, he has worked in the field of electromagnetic compatibility design and testing of high-speed digital signal transmission and high data rate digital systems. His research interests include the EMI and signal integrity issues caused by imbalance of digital high-speed differential transmission lines and other EMI issues related to design of digital computing systems that employ high speed signaling. Prior to joining NCR, he worked for Maxwell Technologies, Inc. and, earlier, IRT Corporation, San Diego, where he held management positions and was engaged in the study and mitigation design of the effects of the electromagnetic pulse created by nuclear weapon detonation, EMI, lightning, and high-powered microwaves on electronic systems. He has authored or presented more than 30 technical papers on topics involving various aspects of electromagnetics and taught more than 20 short courses on electromagnetic pulse effects and electronics survivability both in the United States and in Europe.

Dr. Knighten is a member of Tau Beta Pi, Eta Kappa Nu, and Phi Kappa Phi.

James L. Drewniak (S'85–M'90–SM'01) received the B.S. (with highest honors), M.S., and Ph.D. degrees in electrical engineering from the University of Illinois, Urbana-Champaign in 1985, 1987, and 1991, respectively.

He joined the Electrical Engineering Department, University of Missouri-Rolla, in 1991, where he is part of the Electromagnetic Compatibility Laboratory. His research interests include the development and application of numerical methods for investigating electromagnetic compatibility problems, packaging effects, and antenna analysis, as well as experimental studies in electromagnetic compatibility and antennas.

Dr. Drewniak is an Associate Editor on the IEEE TRANSACTIONS ON ELECTROMAGNETIC COMPATIBILITY.